

# The mass spectrum of metal-free Stars resulting from photodissociation feedback: A scenario for the formation of low-mass population III stars

Kazuyuki Omukai<sup>1,2</sup> and Yuzuru Yoshii<sup>3,4</sup>

omukai@astro.ox.ac.uk; yoshii@ioa.s.u-tokyo.ac.jp

## ABSTRACT

The initial mass function (IMF) of metal-free stars that form in the initial starburst of massive (virial temperatures  $\gtrsim 10^4\text{K}$ ) metal-free protogalaxies is studied. In particular, we focus on the effect of  $\text{H}_2$  photodissociation by pre-existing stars on the fragmentation mass scale, presumedly determined by the Jeans mass at the end of the initial free-fall phase, i.e., at the so-called “loitering phase,” characterized by the local temperature minimum. Photodissociation diminishes the Jeans mass at the loitering phase, thereby reducing the fragmentation mass scale of primordial clouds. Thus, in a given cloud, far ultraviolet (FUV) radiation from the first star, which is supposedly very massive ( $\sim 10^3 M_\odot$ ), reduces the mass scale for subsequent fragmentation. Through a series of similar processes the IMF for metal-free stars is established. If FUV radiation exceeds a threshold level, the star-forming clumps collapse solely through atomic cooling. Correspondingly, the fragmentation scale drops discontinuously from a few time  $10M_\odot$  to sub-solar scales. In compact clouds ( $\lesssim 1.6\text{kpc}$  for clouds of gas mass  $10^8 M_\odot$ ), this level of radiation field is attained, and sub-solar mass stars are formed even in a metal-free environment. Consequently, the IMF becomes bi-modal, with peaks at a few tenths of  $M_\odot$  and a few times  $10M_\odot$ . The high-mass portion of the IMF,  $\xi_{\text{high}}(m_*)$ , is found to be a very steep function of the stellar mass  $m_*$ ,  $\xi_{\text{high}}(m_*) \propto m_*^{-5}$ . Therefore, the typical mass scale of metal-free stars is significantly smaller than that of the very first stars. In the Appendix

---

<sup>1</sup>Department of Physics, Denys Wilkinson Building, Keble Road, Oxford, OX1 3RH, UK

<sup>2</sup>Division of Theoretical Astrophysics, National Astronomical Observatory, Mitaka, Tokyo 181-8588, Japan

<sup>3</sup>Institute of Astronomy, Graduate School of Science, University of Tokyo, Mitaka, Tokyo 181-0015, Japan

<sup>4</sup>Research Center for the Early Universe, Graduate School of Science, University of Tokyo, Bunkyo-ku, Tokyo 113-0033, Japan

we study the thermal instability in collapsing primordial prestellar clumps, and discuss why the thermal instability occurring during the three-body  $\text{H}_2$  formation does not appear to manifest itself in causing further fragmentation of such clumps.

*Subject headings:* cosmology: theory — galaxies: formation — stars: formation

## 1. Introduction

Recent theoretical studies claim that the first stars are very massive, typically about a few times  $10^2 M_\odot$  to  $10^3 M_\odot$ , on the basis that (i) the fragmentation mass scale owing to  $\text{H}_2$  cooling is large, about  $10^3 M_\odot$  (Bromm et al. 1999, 2002; Abel et al. 2000) and (ii) the absence of dust grain formation allows most of the fragment mass to accrete onto a protostar without being halted by stellar radiation feedback (Omukai & Palla 2001, 2003).

The most iron-deficient star yet observed, HE 0107-5240 ( $[\text{Fe}/\text{H}] = -5.3$ ,  $M_* = 0.8 M_\odot$ ; Christlieb et al. 2002), however, presents a puzzle in this regard (see Beers 2003 for a concise summary of the pertinent issues). Shigeyama, Tsujimoto, & Yoshii (2003) suggest that HE 0107-5240 was most probably born as a metal-free Population III star, and has been metal-enriched by accretion of interstellar gas, rather than being born as a Population II star. Whether or not this picture is correct, the very existence of HE 0107-5240 demonstrates that subsolar-mass star formation is possible even in metal-free or extremely metal-poor environments. If HE 0107-5240 was born as a Population II star, the fragmentation mass scale can clearly be reduced to  $\lesssim M_\odot$  as long as a significant amount of metals has been depleted into dust grains (Schneider et al. 2003). Even so, if a completely metal-free star is found in the future, another solution will be required. This possibility has motivated us to examine whether it is feasible to form subsolar-mass stars from primordial gas.

While the first stars were probably very massive, it is important to consider whether *all* metal-free stars must be so massive. Note that metal-free stars might not be exclusively associated with the very first stars, although theoretical studies often make this assumption (e.g., Nakamura & Umemura 2001; Abel et al. 2002; Bromm et al. 2002). The key is that, depending on the nature of Population III stars, the fragmentation process of primordial clouds can be significantly altered owing to stellar feedback, such as the UV radiation field, the kinetic effect of stellar winds and supernovae, etc. In fact, in the presence of a strong far ultraviolet radiation field, metal-free star-forming clumps can collapse solely by atomic cooling, with  $\text{H}_2$  formation prohibited by photodissociation (Nakada & Yoneyama 1976; Hasegawa, Yoshii, & Sabano 1981; Omukai 2001). Then, the fragmentation mass scale can

be reduced to sub-solar scales.

In this paper, we study the evolution of a pregalactic cloud, including its star formation history and the growth of a UV radiation field within it. In particular, we focus on conditions suitable for low-mass star formation, and consider the initial mass function (IMF) of metal-free stars.

Small halos whose virial temperature is less than 8000K cool only by H<sub>2</sub> rotational/vibrational line emission. After the very first episode of star formation, the entire mass of molecular gas is photodissociated by a single or a few massive stars, and subsequent star formation activity is quenched as long as the photodissociating star is present (Omukai & Nishi 1999; Ciardi, Ferrara, Governato, & Jenkins 2000; Glover & Brand 2001; Machacek, Bryan, & Abel 2001). In order for star formation to continue, the pregalactic cloud must be massive enough, i.e., have virial temperature  $> 8000\text{K}$  or correspondingly, a total mass  $\gtrsim 10^8 M_\odot$ . In such clouds, which we consider in this paper, metal-free star clusters will form eventually as a result of successive star formation processes.

The IMF of those metal-free star clusters is of particular importance to the subsequent evolution of the universe, e.g., the metal enrichment, reionization, etc. Consequently, the metal-free stellar IMF has been considered by a number of previous authors. Among them, Yoshii & Saio (1986) studied it in the framework of Silk (1977)’s IMF theory, which assumes the opacity-limited fragmentation scheme of Hoyle (1953), whereby the fragmentation is supposed to continue until the clump becomes optically thick. However, according to recent numerical simulations, the fragmentation mass scale may instead be determined when the isothermality breaks, *before* the opacity becomes important, i.e., at the epoch when the clump temperature begins to increase (Bromm et al. 2002).

By analysing the fragmentation process of filamentary primordial clumps, Nakamura & Umemura (2001) and Bromm et al. (2002) obtained similar estimates for the fragmentation epoch of low-density filaments ( $n_{\text{H}} \lesssim 10^6 \text{cm}^{-3}$ ). Such filaments fragment with masses of a few times  $100 M_\odot$ . Higher density filaments ( $n_{\text{H}} \lesssim 10^{12} \text{cm}^{-3}$ ) fragment, with masses on the order of  $1 M_\odot$ , when the clump becomes optically thick to H<sub>2</sub> lines (see also Uehara et al. 1996; Uehara & Inutsuka 2000). On these grounds, they claimed that the metal-free IMF becomes bi-modal, with peaks around a few times  $100 M_\odot$  and  $1 M_\odot$ , assuming the initial density of filaments are distributed homogeneously up to  $> 10^6 \text{cm}^{-3}$ . However, it is not clear whether the initial densities extend to such high values in realistic situations. Indeed, the 3-D numerical simulations by Abel et al. (2000; 2002) and Bromm et al. (1999; 2002) have not succeeded in producing such low-mass fragments.

Above all, we emphasize that much of the recent work on the metal-free IMF does not

take proper account of feedback effects from already-formed stars. Although various forms of feedback effects can be pointed out, we consider here only the contribution of the FUV radiation field arising from pre-existing stars as a first step toward solution of this problem.

This paper is organized as follows. In §2, the effect of a FUV radiation field on the fragmentation mass scale of primordial gas is discussed. In §3, the evolution of a pregalactic cloud, and the mass spectrum of formed stars are discussed using the result obtained in §2. In §4, a number of important parameters for pregalactic chemical evolution are presented. A brief summary and discussion is then presented in §5. In the Appendix, the possibility of fragmentation due to thermal instability is re-examined.

## 2. Fragmentation of Primordial Gas Clumps in a Far Ultraviolet Radiation Field

In this section, we study the effect of FUV radiation on the fragmentation mass scale of primordial gas. We assume that a pregalactic cloud has an inhomogeneous density structure, consisting of individual “clumps”. As these clumps collapse, they eventually fragment into dense cores (“fragments”) of mass  $m_{\text{frag}}$ . We consider here the evolution of each clump, in particular its fragmentation mass scale.

Although the detailed dynamical evolution of such clumps is rather complex, in general, clumps more massive than several times the Jeans mass are thought to first collapse in a disk-like manner, and subsequently fragment into filamentary clumps (Miyama, Narita, & Hayashi 1987a,b). Finally, with further collapse, the filamentary clumps fragment again into dense cores (Inutsuka & Miyama 1997). All these processes proceed approximately on the free-fall timescale. The density inhomogeneity is amplified by self-gravity in the course of the collapse. The central region experiences run-away collapse, but leaves the outer envelope of lower density unevolved. The size, namely the diameter in the spherical and filamentary case or thickness in the disk case, of the central region is about the Jeans length  $\lambda_J$ , regardless of the shape of the clumps.

The thermal and chemical evolution of primordial clumps irradiated with a FUV radiation has been investigated by Omukai (2001). Here, we use the same model as in Omukai (2001), with minor modifications so that the collapse timescale is changed to the free-fall timescale for the filamentary configuration. Hence, we adopt  $t_{\text{col}} = 1/\sqrt{4G\rho}$  (i.e., Inutsuka & Miyama 1997) rather than the equivalent expression for the spherical case,  $\sqrt{3\pi/32G\rho}$ , where  $\rho$  is the central density of clumps. This change has only a small effect on our results.

The overview of the model is as follows. In this model, the thermal and chemical

evolution for the central region of the clumps is computed. Within the central region, whose length scale is taken as  $\lambda_J/2$ , physical quantities are assumed to be homogeneous. The density increases at the free-fall rate:

$$\frac{d\rho}{dt} = \frac{\rho}{t_{\text{col}}}. \quad (1)$$

The thermal evolution is followed by the energy equation:

$$\frac{dU_{\text{th}}}{dt} = \frac{P}{\rho^2} \frac{d\rho}{dt} - \mathcal{L}_{\text{net}}, \quad (2)$$

where  $U_{\text{th}}$  is the thermal energy per unit mass, and  $P$  is the thermal pressure. The net cooling rate,  $\mathcal{L}_{\text{net}}$ , consists of the contributions from the radiative cooling of atomic hydrogen lines, molecular hydrogen lines, continuum radiation from primordial gas, and the cooling/heating associated with chemical reactions. The optical depth is evaluated by the length scale of the central region  $\lambda_J/2$ . In the case that the clump is optically thick, absorption and scattering effects are taken into account by the escape probability method. The radiation field from outside the clump is also attenuated with the same optical depth. The main effect of radiation field is photodissociation of molecular hydrogen, which is the major coolant in primordial gas clumps. Non-equilibrium chemistry between  $\text{H}$ ,  $\text{H}_2$ ,  $\text{H}^+$ ,  $\text{H}^-$ , and  $\text{H}_2^+$  is solved. Helium is neglected since it is thermally inactive in the considered temperature range. For more details, we refer the interested reader to Omukai (2001).

The radiation field is assumed to be produced only by stars inside the pregalactic cloud, while the possible contributions either from the extragalactic background radiation or from active galactic nuclei are neglected. As discussed §3 below, only very massive ( $40 - 2000 M_\odot$ ) stars are considered as sources of this UV radiation. Since the effective temperature of such massive stars increases only moderately with stellar mass, for simplicity, we assume that the radiation field inside the cloud is approximated by a diluted blackbody at a single temperature  $T_{\text{rad}}$  and take  $T_{\text{rad}} = 10^5 \text{K}$ , which is a typical value of metal-free very massive stars (Ezer & Cameron 1971). Also, the ionizing photons are assumed to be trapped in the HII region formed around the massive stars, and not to contribute to the average radiation field in the protogalaxies. Then, using a parameter  $W$ , the mean intensity can be expressed as

$$J_\nu = W B_\nu(T_{\text{rad}}), \quad (3)$$

for  $h\nu < 13.6 \text{eV}$ , and  $J_\nu = 0$  for  $h\nu > 13.6 \text{eV}$ . The parameter  $W$  is called the dilution factor, hereafter.

Figure 1 shows the temperature evolution of collapsing primordial clumps in the presence of FUV radiation, plotted as a function of the density. The dilution factors,  $W$ , are as

listed in this figure. The initial temperature is taken arbitrarily to be 300K at  $0.1\text{cm}^{-3}$ , because the evolution at higher density, where the fragmentation occurs (at H number density  $n_{\text{H}} \gtrsim 10^4\text{cm}^{-3}$ ), is not affected by this choice.

First, we describe the temperature evolution for primordial clumps without and external radiation field (e.g., Saslow & Zipoy 1967; Matsuda, Sato, & Takeda 1969; Yoneyama 1972; Yoshii & Sabano 1979; Carlberg 1981; Palla, Salpeter, & Stahler 1983; Omukai & Nishi 1998). As seen in Figure 1 (the curve labelled  $W = 0$ ), the temperature of the clump first rises adiabatically, then starts decreasing abruptly by forming sufficient  $\text{H}_2$  for cooling. The temperature decrease stops at  $n_{\text{H}} \sim 10^{2-3}\text{cm}^{-3}$ , where rotational levels of molecular hydrogen reach the local thermodynamic equilibrium. After that, the temperature increases gradually. The actual temperature increase in this phase is slower than shown in Figure 1, owing to the slower collapse rate until the formation of nearly spherical objects by fragmentation. We call this slow collapse epoch the “loitering phase” (e.g., Bromm et al. 2002).

The loitering phase clearly plays a role in the fragmentation of primordial clumps, and has been studied by Bromm et al. (1999, 2002) and Abel et al. (2000, 2002) by way of 3-D hydrodynamical simulation, and by Nakamura & Umemura (2001) by 2-D hydrodynamics assuming that filamentary configurations are formed. According to these studies, the Jeans mass at the loitering phase is imprinted as a typical mass scale for fragmentation. Fragmentation occurs around this point ( $n_{\text{H}} \sim 10^{4-5}\text{cm}^{-3}$ ), and the typical fragment mass scale is the Jeans mass then.

Next, let us see the effect of FUV irradiation on the thermal evolution. Under the presence of a UV radiation field, the formation epoch of  $\text{H}_2$  is delayed until higher densities and temperatures are reached (see Figure 1). The density and temperature at the loitering phase also increase. The net effect of this is to reduce the Jeans mass at the loitering phase. In other words, *the stronger the FUV radiation, the smaller the fragmentation mass scale.*

If the radiation intensity is even more increased, say to the level of  $W > 1 \times 10^{-5}$  in terms of the dilution factor, the photodissociation (for  $n_{\text{H}} \lesssim 10^4\text{cm}^{-3}$ ) and collisional dissociation (for higher densities) prohibit formation of sufficient  $\text{H}_2$  for cooling during the entire prestellar collapse phase. These clumps cool only through atomic radiation processes, namely, H line cooling for  $n_{\text{H}} \lesssim 10^7\text{cm}^{-3}$  and  $\text{H}^-$  bound-free transitions for higher densities (see the evolutionary path for  $W = 1.1 \times 10^{-5}$  in Figure 1). The evolutionary paths for the clumps with  $W > 1.1 \times 10^{-5}$  are almost identical to one another except for the shallow “pit” around  $n_{\text{H}} \sim 10^4\text{cm}^{-3}$  for  $W = 1.1 \times 10^{-5}$ , which disappears in the presence of stronger radiation. An important aspect of the collapse by atomic cooling is that the temperature continues to decrease up to  $n_{\text{H}} \sim 10^{16}\text{cm}^{-3}$ . Consequently, fragmentation occurs at very high density, and sub-solar mass scale fragments are formed.

Next let us evaluate the fragmentation mass scale inferred from the physical conditions at the loitering phase. We define the loitering point as the instance of the temperature minimum around the loitering phase. Fragmentation does not take place immediately at the loitering point. Instead, the clump contracts more, by about 2 orders of magnitude in density (e.g., Nakamura & Umemura 2001), owing to inertia before the fragmentation. Taking this effect into consideration, we evaluate the density and temperature at fragmentation as follows. After the loitering point, the clump is assumed to fragment by contracting 2 orders of magnitude in density. During this period, the temperature is assumed to be constant for molecular cooling clumps, while for atomic cooling clumps the temperature rises (as in Figure 1) because the latter become optically thick before fragmentation. Using the density and temperature at the time of fragmentation, the fragment mass scale is estimated as follows. The wavelength of maximum growing mode for fragmentation is  $\lambda_{\text{mgr}} = 2\pi R_{\text{core}}$ , where the core radius of the filament  $R_{\text{core}} = \lambda_J/2$ . Thus, the typical mass scale for fragments is given by  $m_{\text{frag}} = \rho\pi R_{\text{core}}^2 \lambda_{\text{mgr}}$ , where  $\rho$  is the density at the fragmentation (e.g., Uehara et al. 1996).

In order to collapse and fragment, the mass of the clumps must be more massive than the maximum Jeans mass attained during the collapse. Therefore, only sufficiently massive clumps can give a birth to dense cores and stars, eventually. Probably, in the pregalactic clouds, some clumps satisfy this condition and some do not. Note that, in our model, as long as the clumps are massive enough, the fragmentation mass is only a function of the radiation field since we have adopted the same thermal evolution given in Figure 1 for all those clumps.

Fragmentation mass scales computed in this way are shown in Figure 2 as a function of FUV radiation intensity. In the case of no radiation field ( $W = 0$ ), the fragmentation mass is  $m_{\text{first}} \simeq 2000M_{\odot}$ , which is consistent with the numerical simulations (e.g., Bromm et al. 2002). The fragmentation scale decreases gradually from the initial value  $m_{\text{first}}$  as the radiation intensity increases. When the radiation exceeds the threshold level,  $W_{\text{noH2}} \simeq 1.1 \times 10^{-15}$ , a transition from the  $\text{H}_2$ -cooling triggered collapse to the atomic-cooling one occurs. Correspondingly, the fragmentation scale drops discontinuously from the transition mass,  $m_{\text{tr}} \simeq 40M_{\odot}$ , to sub-solar scales,  $m_{\text{low}} \simeq 0.3M_{\odot}$ .

For an insight into possible values for  $W$ , let us consider here the radiation field at distance  $r$  from a star of radius  $R_*$  and of effective temperature  $T_{\text{eff}}$ . The mean intensity there is

$$J_{\nu} = \frac{R_*^2}{4r^2} B_{\nu}(T_{\text{eff}}). \quad (4)$$

The dilution factor is thus given by

$$W = \frac{R_*^2}{4r^2}. \quad (5)$$

Using the relation  $L = 4\pi R_*^2 \sigma T_{\text{eff}}^4$ , and noting the luminosity of massive stars  $L$  is close to  $L_{\text{Edd}}$ , the dilution factor can be expressed as

$$W = 3 \times 10^{-15} \left( \frac{T_{\text{eff}}}{10^5 \text{K}} \right)^{-4} \left( \frac{m_*}{50 M_\odot} \right) \left( \frac{r}{3 \text{pc}} \right)^{-2} \left( \frac{L}{L_{\text{Edd}}} \right), \quad (6)$$

where  $m_*$  is the mass of the star. Then, if the massive stars ( $\gtrsim 50 M_\odot$ ) are predominantly formed and their mean separation is  $\sim$  a few pc, the threshold level  $W_{\text{noH}_2} \simeq 1.1 \times 10^{-15}$  can be reached. In §3, we discuss whether this level of radiation field is reached during the evolution of pregalactic clouds.

In this paper we assume that the dense clumps formed by fragmentation around the loitering phase do not produce sub-fragments. The possibility of sub-fragmentation due to thermal instability has been claimed by some authors (Sabano & Yoshii 1977; Yoshii & Sabano 1979; Silk 1983; Yoshii & Saio 1986). In the Appendix, we re-examine this question via a linear perturbation analysis of the gravitationally collapsing primordial gas. Although the thermal instability does occur in the active phase of the three-body  $\text{H}_2$  formation reaction, the instability remains weak and does not appear to cause further fragmentation of the clumps. Therefore, we do not consider the sub-fragmentation by the thermal instability in the following.

### 3. Star Formation in Pregalactic Clouds and Establishment of the Stellar Mass Spectrum

In §2 we discussed the evolution of subclumps in a pregalactic cloud, and obtained the fragmentation mass scale as a function of the FUV radiation intensity. Here, let us consider the evolution of pregalactic clouds as a whole. The history of the build-up of the stellar radiation field and the consequent IMF within a pregalactic cloud is examined. As discussed in §2, sub-solar mass stars are formed if the FUV radiation field exceeds the threshold level, which is  $W_{\text{noH}_2} \simeq 10^{-15}$  in terms of the dilution factor. The condition of the cloud when this transition actually occurs is also examined.



### 3.1. A Model for Pregalactic Clouds

Suppose that pregalactic clouds consist of two-phase medium, i.e., diffuse gas and denser clumps. The clumps collapse and form stars eventually, as described in §2. Since the physical condition of the clumps, e.g., initial density, temperature, etc., varies from clumps to clumps, the star formation epoch in those clumps would differ each other. The star formation rate in clumps, local radiation field, and other local quantities, do depend on the local condition in the clumps. Here for simplicity, we assume that the quantities averaged over the entire cloud, e.g., the averaged star formation rate, are controlled by averaged global quantities of the cloud, e.g., the averaged gas density. Specifically, we use a one-zone model of pregalactic clouds, where the physical quantities such as the gas density,  $\rho_{\text{gas}}$ , stellar density,  $\rho_*$ , and stellar radiation field,  $u_{\text{rad}}$ , are taken to be averaged values (see e.g., Yoshii & Saio 1985).

Let the initial gas mass be  $M_{\text{cl}}$ , and the length scale be  $l$ . The initial gas density is given by

$$\rho_{\text{gas}}(0) = \frac{M_{\text{cl}}}{l^3}. \quad (7)$$

The length scale of the cloud  $l$  is assumed to be constant in time. While the fragments themselves continue their own collapse, the parental pregalactic cloud is kept in dynamical equilibrium by the kinetic energy of the fragments.

The basic assumptions of this model are (i) star formation proceeds on the free-fall timescale, and (ii) the stellar mass scale coincides with the fragmentation scale, which is a function of the radiation intensity, using the relation in Figure 2.

The average gas density,  $\rho_{\text{gas}}$ , in the cloud is followed by

$$\frac{d\rho_{\text{gas}}}{dt} = -\frac{\rho_{\text{gas}}}{t_{\text{sf}}}. \quad (8)$$

For the star formation timescale,  $t_{\text{sf}}$ , we take the free-fall timescale,  $t_{\text{col}} = 1/\sqrt{4G\rho_{\text{gas}}}$ . We neglect the recycling of gas ejected by either supernovae or stellar winds, assuming that it directly escapes from the cloud. Also, gas is always assumed to be primordial and chemical enrichment effects are not taken into account, since we are now interested only in metal-free stars.

Let the number of stars per unit volume at time  $t$  in mass range  $dm_*$  be  $\xi(m_*, t)dm_*$ . By summing up the radiation from all stars, the average radiation energy density in the cloud is given by

$$u_{\text{rad}} = \frac{l}{c} \int \xi(m_*, t) L(m_*) dm_*. \quad (9)$$

The values of luminosity  $L(m_*)$  of a Population III star with mass  $m_*$  are taken from Schaerer (2002). Here, the radiation spectrum is supposed to be a diluted blackbody of  $T_{\text{rad}} = 10^5 \text{K}$ , since we consider the radiation from massive metal-free stars ( $> m_{\text{tr}} \simeq 40 M_{\odot}$ ). The mass scale of fragmentation at time  $t$ ,  $m_{\text{frag}}(t)$ , is determined by  $u_{\text{rad}}(t)$  by the relation shown in Figure 2. Stars are assumed to turn off after their main sequence lifetimes. Here, the main sequence lifetime of stars without stellar wind given by Schaerer (2002) is used. For stellar masses higher than  $500 M_{\odot}$ , whose lifetime is not given in the literature, the same lifetime as that for  $500 M_{\odot}$  is used.

With the above assumptions, the equation for stellar number density,  $\xi(m_*, t)$ , is formally written as

$$\frac{\partial \xi(m_*, t)}{\partial t} = \frac{\rho_{\text{gas}}}{m_{\text{frag}} t_{\text{sf}}} \delta(m_* - m_{\text{frag}}) - \xi(m_{\text{d}}, t_{\text{d}}) \left| \frac{dm_{\text{d}}}{dt} \right| \delta(m_* - m_{\text{d}}), \quad (10)$$

where  $m_{\text{d}}$  is the mass of stars that dies at time  $t$ , and  $t_{\text{d}}$  is their formation time, hence  $t_{\text{d}} = t - t_*(m_{\text{d}})$ . In the equation above, the first term on the right hand side is the star formation rate, and the second term is the stellar death rate. Equations (8) and (10) are integrated until  $\rho_{\text{gas}}$  falls below 10 % of the initial value,  $\rho_{\text{gas}}(0)$ , or the FUV radiation exceeds the threshold value for atomic-cooling collapse, for which we use the threshold dilution factor  $W_{\text{noH}_2} = 1 \times 10^{-15}$ . Note again that this is still a qualitative, rather than a quantitative, approach to study early star formation in pregalactic clouds, and it is of course not realistic that only 10 % of the initial gas remains into the ISM. The evolution of pregalactic clouds is not affected by this value: only the termination epoch of the calculation is changed.

### 3.2. The Conditions for Low-Mass Star Formation

Two cases of cloud mass  $M_{\text{cl}}$  are studied: (a)  $M_{\text{cl}} = 10^7 M_{\odot}$ , and (b)  $10^8 M_{\odot}$ . For case (a), the length scale,  $l$ , is varied from 100 to 1000 pc, while for case (b),  $l = 300 - 3000$  pc. The evolution of the average radiation field,  $u_{\text{rad}}$ , is presented in Figures 3 (for case a) and 4 (for case b).

We see in Figures 3 and 4 that the radiation field in relatively compact clouds, whose length scale  $l \leq 500 \text{pc}$  for  $M_{\text{cl}} = 10^7 M_{\odot}$  or 1000 pc for  $M_{\text{cl}} = 10^8 M_{\odot}$ , reaches the critical level for low-mass star formation, while it does not in more diffuse ones. In pregalactic clouds

where low-mass stars are formed, the value of  $W$  is expected to remain at the threshold level  $W_{\text{noH}_2}$  until early-formed massive stars begin to die about  $t \simeq 2 \times 10^6 \text{ yrs}$ , since low-mass stars do not emit FUV radiation. On the other hand, in larger clouds the radiation energy density  $u_{\text{rad}}$  fails to reach the critical level  $u_{\text{noH}_2} = W_{\text{noH}_2} a T_{\text{rad}}^4$ , and declines after the first stars begin to turn off. In other words, there is a threshold cloud length,  $l_{\text{th}}$ , below which the radiation intensity reaches the critical value. This threshold length is larger for the cloud of  $10^8 M_{\odot}$  ( $l_{\text{th}} > 1000 \text{ pc}$ ) than for that of  $10^7 M_{\odot}$  ( $l_{\text{th}} < 1000 \text{ pc}$ ).

We now discuss analytically the behavior of the radiation field and the threshold cloud length. For simplicity, we suppose that the gas depletion timescale,  $t_{\text{dep}} \simeq t_{\text{sf}}(0)$ , is longer than the lifetime of the first star,  $t_*(m_{\text{first}})$ . A similar discussion holds in the opposite case with some modification. Also, since the stellar lifetime and luminosity-to-mass ratio is only weakly dependent on mass for massive stars, in the following analytical discussion we use a constant value of  $t_{*,\text{high}} = 2 \times 10^6 \text{ yr}$  and  $(L/M)_* = 3 \times 10^4 (L/M)_{\odot}$ , which are the values for a star of  $1000 M_{\odot}$ , for all massive stars ( $> m_{\text{tr}}$ ).

Before significant gas depletion takes place, at  $t < t_{\text{dep}}$ , the average gas density  $\rho_{\text{gas}} \simeq \rho_{\text{gas}}(0)$  and the star formation rate is approximately constant at  $\rho_{\text{gas}}(0)/t_{\text{sf}}(0)$ . The stellar mass density is

$$\rho_*(t) \simeq \begin{cases} \rho_{\text{gas}}(0)t/t_{\text{sf}}(0) & t < t_{*,\text{high}}, \\ \rho_{\text{gas}}(0)t_{*,\text{high}}/t_{\text{sf}}(0) & t_{*,\text{high}} < t < t_{\text{dep}}. \end{cases} \quad (11)$$

After the gas is depleted significantly, the star formation rate drops to  $\rho_{\text{gas}}(t)/t_{\text{sf}}(t)$ . Thus

$$\rho_*(t) \simeq \rho_{\text{gas}}(t)t_{*,\text{high}}/t_{\text{sf}}(t) \quad t > t_{\text{dep}}. \quad (12)$$

By the way, the radiation density is given by

$$u_{\text{rad}}(t) = \frac{l}{c} \rho_*(t) (L/m)_*, \quad (13)$$

as long as all the stars are massive, namely  $u_{\text{rad}} < u_{\text{noH}_2}$ . Since  $(L/m)_*$  is only weakly dependent on  $m_*$ , the radiation field is proportional to the stellar mass density  $\rho_*$ . Therefore, the radiation intensity first increases linearly in time ( $t < t_{*,\text{high}}$ ), then remains constant ( $t_{*,\text{high}} < t < t_{\text{dep}}$ ), and finally declines as the gas in the cloud depletes ( $t > t_{\text{dep}}$ ).

The radiation dilution factor  $W$ , which is related to the radiation energy density  $u_{\text{rad}}$  by  $W = u_{\text{rad}}/7.56 \times 10^5 (\text{erg/cm}^3)$ , is

$$W = 0.5 \times 10^{-14} \left( \frac{l}{1\text{kpc}} \right)^{-7/2} \left( \frac{M_{\text{cl}}}{10^8 M_{\odot}} \right)^{3/2} \left( \frac{t}{2 \times 10^6 \text{yr}} \right) \quad (t < t_{*,\text{high}}), \quad (14)$$

and reaches maximum at  $t = t_{*,\text{high}}$ . Therefore, only in clouds whose length scale is smaller than the threshold length

$$l_{\text{th}} = 1.6\text{kpc} (M_{\text{cl}}/10^8 M_{\odot})^{3/7}, \quad (15)$$

the dilution factor  $W$  reaches  $W_{\text{noH}_2} \simeq 1 \times 10^{-15}$ , and sub-solar mass stars are formed thereafter. This value of  $l_{\text{th}}$  agrees well with the numerical result presented in Figures 3 and 4.

The number of low-mass stars formed can be estimated by the following considerations. Since low-mass stars do not emit UV radiation,  $u_{\text{rad}}$  remains constant after reaching  $u_{\text{noH}_2}$  at  $t = t_{\text{lmsf}}$ , where

$$t_{\text{lmsf}} = 4 \times 10^5 \text{yr} \left( \frac{l}{1\text{kpc}} \right)^{7/2} \left( \frac{M_{\text{cl}}}{10^8 M_{\odot}} \right)^{-3/2}, \quad (16)$$

until the massive stars start to die at  $t = t_{*,\text{high}}$ . Then, the duration of low-mass star formation is  $t_{*,\text{high}} - t_{\text{lmsf}}$ . Multiplying by the star formation rate, the mass density of low-mass stars is

$$\rho_{*,\text{low}} = \frac{\rho_{\text{gas}}(0)}{t_{\text{sf}}(0)} (t_{*,\text{high}} - t_{\text{lmsf}}). \quad (17)$$

Metal-free star formation continues for the duration  $\Delta t = t_{*,\text{high}}$ , i.e., from the first star formation until the massive stars begin to explode as supernovae. At time  $t = t_{\text{lmsf}}$  in this period, low-mass star formation starts. Since the star formation rate is approximately constant at  $\rho_{\text{gas}}(0)/t_{\text{sf}}(0)$ , the mass fraction of metal-free stars that is locked into low-mass stars is given by the ratio of the two durations:

$$f_{\text{low}} = \frac{\rho_{*,\text{low}}}{\rho_{*,Z=0}} = \frac{t_{*,\text{high}} - t_{\text{lmsf}}}{t_{*,\text{high}}} \quad (18)$$

$$= 1 - \left( \frac{l}{l_{\text{th}}} \right)^{7/2} \quad (19)$$

$$= 1 - 0.2 \left( \frac{l}{1\text{kpc}} \right)^{7/2} \left( \frac{M_{\text{cl}}}{10^8 M_{\odot}} \right)^{-3/2}, \quad (20)$$

where  $\rho_{*,Z=0}$  is the density of metal-free stars.

### 3.3. The Stellar Initial Mass Function

Because of the mass gap between low-mass stars ( $\simeq 0.3M_{\odot}$ ) and high-mass stars ( $\gtrsim 40M_{\odot}$ ), the metal-free IMF becomes bi-modal.

In our idealized model, the low-mass IMF is delta-function-like: only stars of  $m_{\text{low}} \simeq 0.3M_{\odot}$  are formed (see Figure 2). Actually, a distribution of the fragmentation mass around this value would be present. Competitive accretion of ambient gas would create some distribution of the protostellar mass. Also, the coagulation between fragments might form more massive cores. As a result of these processes, the low-mass IMF would be formed, although we do not discuss it further here. Recall that the peak ratio between the high and low-mass IMF can be obtained by the mass fraction of low-mass stars  $f_{\text{low}}$  given by equation (20).

On the other hand, the high-mass IMF,  $\xi_{\text{high}}(m_*)$ , of metal-free stars that are more massive than the transition mass  $m_{\text{tr}} \simeq 40M_{\odot}$  has been obtained in our model, and is shown in Figure 5 for clouds of  $M_{\text{cl}} = 10^8 M_{\odot}$  (case a). In three cases of  $l = 300, 500$ , and  $1000\text{pc}$ , the shape of the IMF is identical, and the value of IMF at the same mass is proportional to  $l^{-1}$ . In the case of  $l = 3\text{ kpc}$ , the radiation field does not reach the threshold value, and no low-mass stars are formed (see Figure 4). In this case, the instantaneous mass of forming stars first reaches a minimum of  $140M_{\odot}$  and then increases as the radiation intensity declines. The stars of  $m_* \lesssim 300M_{\odot}$  can be produced at two different epochs, first when the radiation density is increasing and second when the radiation density is decreasing. The stars formed at different epochs are shown separately in Figure 5. The actual IMF is the sum of them.

We now present an analytic derivation of the high-mass IMF,  $\xi_{\text{high}}$ , following Silk (1977). Here, we consider stars formed at  $t < t_*(m_{\text{first}})$ , namely, during the time when the first star is still alive, as those formed later are probably metal-polluted. Thus, the maximum mass of existing stars is just the mass of the first star,  $m_{\text{first}}$ . The radiation energy density at time  $t$  is given by

$$\frac{u_{\text{rad}}(t)}{l/c} = \int_{m_*(t)}^{m_{\text{first}}} \xi_{\text{high}}(m'_*) L(m'_*) dm'_*, \quad (21)$$

where  $m_*(t)$  is the mass of forming star at  $t$ . Differentiating both sides of the equation (21) with  $m(t)$ , we obtain the mass spectrum

$$\xi_{\text{high}}(m_*) = \frac{c}{lL(m_*)} \left| \frac{du_{\text{rad}}}{dm_*} \right|. \quad (22)$$

Suppose now the relations  $u_{\text{rad}} \propto m_*^\alpha$  and  $L \propto m_*^\beta$ . In this case, the IMF becomes

$$\xi_{\text{high}} \propto m_*^{\alpha-\beta-1}. \quad (23)$$

This relation was first derived by Silk (1977). From Figure 2, the approximate relation between fragmentation mass and radiation density,  $m_{\text{frag}} \propto W^{-1/3}$ , holds for massive stars of  $m_* \sim 100M_\odot$ . For these massive stars, the luminosity-mass relation  $L \propto m_*$  holds. Then, it follows that  $\alpha = -3$  and  $\beta = 1$  for those stars. Substituting these values into relation (23), we finally obtain the metal-free IMF for massive stars:

$$\xi_{\text{high}} \propto m_*^{-5}. \quad (24)$$

The mass spectrum becomes a very steep function of mass because of the negative value of  $\alpha$ . The normalization constant for the relation (24) depends on the length scale of the pregalactic cloud as  $\propto l^{-1}$ , as seen in equation (21). Thus, using the values in Figure 5, the IMF can be expressed approximately as

$$\xi_{\text{high}} = 3 \times 10^{-6} (\text{stars } M_\odot^{-1} \text{ pc}^{-3}) \left( \frac{l}{1 \text{ kpc}} \right)^{-1} \left( \frac{m_*}{50M_\odot} \right)^{-5}. \quad (25)$$

Note that the IMF is independent of the mass of the pregalactic cloud (see eq. 21). Also the transition mass  $m_{\text{tr}} \simeq 40M_\odot$  does not depend on the cloud mass because this comes from the discontinuity in the  $m_{\text{frag}} - W$  relation (Figure 2), which is independent of the cloud mass.

A bi-modal IMF for metal-free stars has also been proposed also by Nakamura & Umemura (2001), as mentioned in §1. It is interesting to note here the differences between our IMF and theirs. They pointed out that the IMF becomes bi-modal, with peaks around 1 and 100  $M_\odot$ , if dense ( $n_{\text{H}} > 10^6 \text{ cm}^{-3}$ ) filamentary clumps formed in the course of collapse. It is, however, still uncertain that such dense filaments are formed in reality. On the other hand, we consider here only the low-density filaments that fragment initially during the loitering phase. Even so, the sub-solar mass peak appears, owing to photodissociation feedback from pre-existing stars. Recall also that the production mechanism of the low-mass stars is different in the two treatments. Nakamura and Umemura (2001) considered fragmentation of dense molecular-cooling clouds around  $n_{\text{H}} \simeq 10^{12} \text{ cm}^{-3}$ , while we considered fragmentation of atomic-cooling clouds around  $n_{\text{H}} \simeq 10^{16} \text{ cm}^{-3}$ .

#### 4. Metal Enrichment by First-Generation Stars

The chemical enrichment by the first-generation stars has particular importance for the subsequent chemical evolution of protogalaxies. Also, the masses of those stars can be constrained by observing the abundance ratios of elements in second-generation stars. In §3, the IMF for metal-free stars was predicted to be bi-modal with peaks around  $0.3M_\odot$  and  $40M_\odot$ . In this section, we discuss the chemical yield of the first-generation stars under the predicted IMF.

Since low mass stars do not eject metals (until after completing their long lifetimes), we do not need to know the detailed shape of the low-mass IMF. The mass ratio of low-mass stars,  $f_{\text{low}}$ , given by equation (20), suffices for our purpose. For simplicity, we approximate the high-mass portion of IMF as

$$\xi_{\text{high}} \propto m_*^{-5} \quad (m_{\text{tr}} < m_* < m_{\text{first}}) \quad (26)$$

in this section. We define the mean mass fraction of ejected element  $X$  by supernovae

$$\epsilon_{X,\text{high}} = \int dm_* m_X \xi_{\text{high}} / \int dm_* m_* \xi_{\text{high}}, \quad (27)$$

and the mean remnant mass fraction

$$\alpha_{\text{high}} = \int dm_* m_{\text{rem}} \xi_{\text{high}} / \int dm_* m_* \xi_{\text{high}}. \quad (28)$$

Using these quantities, the yield of element  $X$  by the first-generation stars is expressed as

$$p_X = \frac{\epsilon_{X,\text{high}}(1 - f_{\text{low}})}{f_{\text{low}} + (1 - f_{\text{low}})\alpha_{\text{high}}}. \quad (29)$$

Considering the uncertainty of the transition mass,  $m_{\text{tr}}$ , we calculate the yield for two cases of  $m_{\text{tr}} = 20$  and  $40M_\odot$ , respectively. We fix  $m_{\text{first}} = 2000M_\odot$  since the uncertainty of this causes little difference owing to the steepness of IMF. The values of  $\epsilon_{X,\text{high}}$  and  $\alpha_{\text{high}}$  are presented in Tables 1 and 2 for  $m_{\text{tr}} = 20$  and  $40M_\odot$ , respectively. We use the Population III supernova (SN) yields by Umeda & Nomoto (2002). Metals are ejected by stars in the mass range  $13 - 30M_\odot$  by Type II SNe, and  $150 - 270M_\odot$  by pair-instability SNe. Metal-free stars whose mass is between these ranges, as well as those more massive than  $270M_\odot$ , collapse into black holes with little metal ejection. Since the fraction of gas returning to the interstellar

medium is quite uncertain, we assume here that all of the stellar material is eventually locked into black holes in this mass range.

A comparison of predicted elemental abundance ratios with the observed most iron-deficient star HE 0107-5240 (Christlieb et al. 2002) is shown in Table 3. When the cutoff mass,  $m_{\text{tr}}$ , is higher than  $30M_{\odot}$ , metal enrichment proceeds only via pair-instability SNe, and the abundance ratios become identical to this single source. Christlieb et al. (2002) claimed that a Type II SN of a  $20 - 25M_{\odot}$  metal-free star reproduces the observed abundance pattern heavier than Mg, while lighter elements could be accounted for by self-enrichment or mass transfer from a more massive AGB companion star. On the other hand, Schneider et al. (2003) pointed out that the abundance pattern from a pair-instability SN of a  $200 - 220M_{\odot}$  star also agrees with the limited number of elemental abundances presently available for this star. So far, the enrichment either by Type II or by pair-instability SNe seems to be consistent with the observed abundance ratios. As a result, the abundance pattern of HE 0107-5240 heavier than Mg is well-reproduced in all cases shown in Table 3 within 0.2-0.3 dex, although in the case of  $m_{\text{tr}} > 30M_{\odot}$  the amount of Mg relative to Fe might be too small.

Recently, Umeda & Nomoto (2003) proposed the “mixing and fallback” scenario: the processed material is assumed to be mixed uniformly in the region from  $1.8M_{\odot}$  to  $6.0M_{\odot}$ , and almost all material in this layer falls back to the central remnant; only a small fraction is ejected from this region. Although this beautifully explains the abundance ratios of HE 0107-5240, including the large C and O abundances relative to Fe, this theory contains unknown free parameters, namely the extent of mixing and the mass-cut.

Note, however, that we do not take it as yet established that HE 0107-5240 is a second-generation star formed from metal-enriched material. We stress here that since sub-solar mass stars can form in a metal-free environment, HE 0107-5240 might be a first-generation star metal-polluted due to subsequent accretion (Yoshii 1981; Shigeyama et al. 2003). The large  $[\text{C}/\text{Fe}] (= +4.0)$  ratio of HE 0107-5240, as well as the large  $[\text{O}/\text{Fe}] (= +2.4)$  ratio (private communication; M. S. Bessell), can be explained by the self-enrichment in the AGB phase (private communication M. Y. Fujimoto; Fujimoto, Ikeda, & Iben 2000). The accretion scenario demonstrates that the gap in the metallicity distribution function of observed low-metallicity stars, between  $[\text{Fe}/\text{H}] = -5.3$  and the current lower limit  $[\text{Fe}/\text{H}] = -3.5$  to  $-4.0$  of extreme metal-poor stars could be real, as shown in Figure 2 of Shigeyama et al. (2003).

On the other hand, if the explosion of massive metal-free stars was responsible for the birth of the  $[\text{Fe}/\text{H}] = -5.3$  star as a second-generation star (Schneider et al. 2003; Umeda & Nomoto 2003; Bonifacio, Limongi, & Chieffi 2003), there must exist many more second-generation stars having a wide variety of metal abundances below  $[\text{Fe}/\text{H}] = -3.5$ . Therefore, this massive Population III scenario prefers the existence of a metallicity distribution without



any appreciable gap below  $[\text{Fe}/\text{H}]=-3.5$ , and future large samples of extremely metal-poor stars will clearly discriminate between the competing scenarios proposed thus far.

## 5. Summary and Discussion

We have studied the initial mass function (IMF) of the first-generation stars under the assumption that the fragmentation of prestellar clumps occurs around the “loitering phase,” i.e., when the temperature stops decreasing. The fragmentation mass scale decreases as the far ultraviolet radiation field becomes intense. If the very first stars are very massive and create intense radiation fields inside their parent clouds, stars formed later are smaller than those formed earlier. The stellar initial mass function is established by this mechanism. Low-mass star formation occurs only in clouds whose length scale  $l$  is less than the threshold length  $l_{\text{th}} \simeq 1.6\text{kpc}(M_{\text{cl}}/10^8 M_{\odot})^{3/7}$ , where  $M_{\text{cl}}$  is the initial gas mass of the cloud. In such clouds, the IMF becomes bi-modal: the high-mass peak is about  $40M_{\odot}$  and the low-mass one locates at about  $0.3M_{\odot}$ . Numerous low-mass metal-free stars are formed, greatly exceeding the number of massive metal-free stars. The high-mass portion of the IMF is found to be  $\xi_{\text{high}} = 3 \times 10^{-6}(\text{stars } M_{\odot}^{-1} \text{ pc}^{-3})(l/1\text{kpc})^{-1}(m_*/50M_{\odot})^{-5}$ , which is a very steep function of stellar mass  $m_*$ , with a power-law index of  $-5$ , in comparison with the Salpeter IMF’s index of  $-2.35$ . Thus, although the very first stars are possibly very massive,  $\sim 1000M_{\odot}$ , the typical mass scale for metal-free stars is smaller, and depends on the length scale of the pregalactic clouds.

If all metal-free stars were indeed as massive as the very first stars, they would evolve to black holes without metal ejection. The surrounding gas remains metal-free, and the very massive star formation mode continues indefinitely. This is the so-called *star formation conundrum* pointed out by Schneider et al. (2002). Our scenario, where the UV radiation from the preceding stars allows production of low-mass stars from metal-free gas, might provide a solution to this conundrum.

Recently, Mackey, Bromm, & Hernquist (2003) studied the star formation history in the high-redshift universe, in particular the transition from Population III to Population II star formation. They assumed that the same top-heavy IMF is maintained not only in low-mass halos that cool only via molecular cooling, but also in halos that are massive enough to cool via atomic hydrogen lines. According to our results, however, the mass scale of stars that form in massive halos is smaller than those that form in low-mass halos.

We now understand that low-mass star formation occurs in a primordial cloud only if the radius of the cloud is below the threshold  $l_{\text{th}} \simeq 1.6\text{kpc}(M_{\text{cl}}/10^8 M_{\odot})^{3/7}$ . We should

ask whether this is the case in reality. The virial radius of a pregalactic cloud,  $r_{\text{vir}} \simeq 2\text{kpc}(M_{\text{cl}}/10^8 M_{\odot})^{1/3}(1 + z_{\text{vir}}/20)^{-1}$ , that collapses at redshift  $z_{\text{vir}}$  should be regarded as the maximum radius of the cloud, since it cools and contracts after virialization to reach dynamical equilibrium as a whole. Comparing  $l_{\text{th}}$  and  $r_{\text{vir}}$ , we conclude that pregalactic clouds with  $l < l_{\text{th}}$  are not rare objects. Therefore, *sub-solar mass metal-free stars are generically formed in the framework of standard cosmology. If metal-free low-mass stars are not be found in the Galactic halo, an exotic scenario for structure formation must be invoked.*

Our model for pregalactic clouds is obviously oversimplified, and should therefore be improved upon before the above conclusion is taken for granted. In the following, we summarize our assumptions and their limitations. More elaborate works taking these points into account are desirable in future studies.

- We have used a one-zone model for pregalactic clouds. Inhomogeneity inside a pregalactic cloud is not taken into account. In particular, we have assumed that the star formation timescale is given by the averaged free-fall time. Of course, the evolution of pregalactic clouds and initial mass function of first-generation stars crucially depend on this assumption. Although this assumption has not been fully justified, there are some observational suggestions that the global star formation rate (SFR) in galaxies is indeed determined by galactic scale conditions (e.g., Kennicutt 1998).

First, we consider the effect of the spatial fluctuations of SFR within the pregalactic cloud. If the star formation is very active in a region in comparison with the rest of the cloud, this star-forming region itself can be regarded as an almost independent cloud. Since the length scale of the star-forming region is smaller than that of the entire cloud, this allows easier build-up of local radiation field and easier low-mass star formation.

Next, we discuss the effects of different values of the global SFR. Possible changes in the averaged SFR do not affect the high-mass IMF directly, since the equation (22) does not contain the SFR. On the other hand, the condition for low-mass star formation discussed in §3.2 will be altered. If the star formation process is slower than that assumed here, the radiation field will increase more slowly. This results in a smaller value of the threshold length  $l_{\text{th}}$  for low-mass star formation than in equation (15).

- We have only considered the averaged radiation field and have neglected its local fluctuations. In reality, the radiation field is stronger in a region closer to a massive star than in outer regions. Therefore, dispersion around the average fragmentation scale must exist at any time. This effect might affect the IMF in the pregalactic clouds.

- We have derived the fragmentation mass scale from the condition at the local temperature minimum, or “loitering point”. Because of this simplified treatment, the value of fragmentation mass scale should be regarded as precise only in the order-of-magnitude sense. More accurate determination of fragmentation mass scale under UV radiation field is an interesting topic for future studies (see e.g., Bromm & Loeb 2003; Yoshida et al. 2003). Also, the fragmentation epoch depends on the initial density and line-mass of filaments (Nakamura & Umemura 2001). The dense and large line-mass filaments collapse until very high density ( $10^{12}\text{cm}^{-3}$ ) without fragmenting. It is important to specify these properties of filaments in the realistic cosmological context.
- We have assumed that the stellar mass scale coincides with the fragmentation scale. If the accretion rate drops suddenly for massive protostars, as suggested by Abel et al. (2002), the stellar mass scale falls short of the fragmentation scale. This depends crucially on the late-time behavior of the accretion rate, which has not yet been fully explored.
- We have assumed that the ionizing photons are trapped in the HII region formed around the massive stars, and do not contribute to the average radiation field in the protogalaxies. This assumption depends on the size and distribution of the HII regions. From comparison of the results by Susa & Kitayama (2000) and Omukai (2001), we expect that the thermal evolution does not deviate so much from those we used in §2 even if the ionizing photons are included. Therefore, even if this assumption is invalidated, the results will not be altered significantly.
- We have neglected kinematical effects of the HII regions formed around massive stars. If either the density around the star or the protostellar accretion rate is sufficiently high, the HII region is confined to a small region around the exciting star. If not, the HII region expands due to high internal pressure, and the entire pregalactic cloud might be disrupted by photoevaporation. If the pregalactic clouds are disk-like, an HII region extends preferentially in the vertical direction to the disk, and it ends up with a hole like a chimney (Franco, Tenorio-Tagle, & Bodenheimer 1990). Therefore, even if photoevaporation by massive stars occurs, it may not be sufficiently violent to disrupt the entire pregalactic cloud. However, more thorough studies are necessary to draw this conclusion with confidence.
- We have assumed that formed stars start shining as main sequence stars immediately. Stars are, however, formed by protostellar accretion, and the accretion phase precedes the main-sequence phase. If the mass accretion rate is  $\dot{m}_{\text{acc}}$ , the duration of accretion phase for a star of mass  $m_*$  is  $t_{\text{acc}} = m_*/\dot{m}_{\text{acc}}$ . In the case of primordial star formation, the accretion rate is very high:  $10^{-2} - 10^{-3} M_{\odot}/\text{yr}$  (Stahler, Palla, & Salpeter 1986;

Omukai & Nishi 1998). Then, the accretion phase is short in comparison with the stellar lifetime. However, for the most massive stars ( $\lesssim 1000M_{\odot}$ ), the accretion phase lasts for a significant part of the expected stellar lifetime. For such high accretion rate, the accretion flow becomes optically thick to  $H^{-}$  bound-free absorption. The effective temperature,  $T_{\text{eff}}$ , of accreting protostars is about 6000K, while at the main-sequence stage it becomes  $T_{\text{eff}} \simeq 10^5 K$  (Stahler et al. 1986; Omukai & Palla 2001, 2003). Thus, if the accretion phase is prolonged, the emitted FUV radiation decreases significantly.

- We have assumed that the star formation timescale is similar to the free-fall time of the cloud. In other words, we considered only the spontaneous mode of star formation. Triggered star formation by stellar winds or SNe (Elmegreen & Lada 1977) has not been included in our model, since both stellar winds or pulsational mass losses are expected to be rather weak for metal-free stars (Kudritzki 2000; Baraffe, Heger, & Woosley 2001).

We thank Tim Beers for careful reading of the manuscript and the referee, Benedetta Ciardi, for comments that improved the presentation of the paper. This work is supported in part by Research Fellowship of the Japan Society for the Promotion of Science for Young Scientists (6819; KO), and the Grant-in-Aid for Scientific Research (1520401) and Center-of-Excellence Research (07CE2002) from Ministry of Education, Culture, Sports, Science, and Technology (YY).

### A. Thermal Instability in Collapsing Metal-Free Clumps

In this appendix, we study the thermal-chemical instability using a linear perturbation theory, following Sabano & Yoshii (1977) and Yoshii & Sabano (1979). The energy equation (A1) and the equation of H<sub>2</sub> formation/dissociation (A6) are perturbed under the isobaric condition  $\delta P = 0$ . The energy equation is

$$\frac{dU}{dt} - \frac{P}{\rho} \frac{d \ln \rho}{dt} = -\mathcal{L} \quad (\text{A1})$$

where  $U$  is the internal energy per unit mass, including the thermal and chemical binding energy

$$U = \frac{3}{2} \frac{k_B T}{\mu_a m_H} - \frac{1}{2} \frac{\chi f}{m_H}, \quad (\text{A2})$$

and  $\mathcal{L} = \mathcal{L}_{\text{H}_2}$  is the cooling rate by H<sub>2</sub> line emission. In equation (A2),  $f$  is the molecular fraction <sup>5</sup>, and  $\chi$  is the chemical binding energy of H<sub>2</sub>. Note that, unlike in §2, the cooling rate  $\mathcal{L}$  does not include chemical cooling/heating. Instead, the definition of the internal energy  $U$  is modified to include the chemical binding energy. The equation of state for an ideal gas is used:

$$P = \frac{\rho k_B T}{\mu m_H}. \quad (\text{A3})$$

In the equations above,

$$\mu^{-1} = 1 - \frac{f}{2}, \quad (\text{A4})$$

and

$$\mu_a^{-1} = 1 - \frac{3\gamma_{\text{H}_2} - 4}{\gamma_{\text{H}_2} - 1} \frac{f}{3} = 1 - \frac{f}{6}, \quad (\text{A5})$$

where the adiabatic index for molecular hydrogen,  $\gamma_{\text{H}_2} = 7/5$ , has been used, and the electron fraction,  $x_e$ , has been assumed to be small,  $x_e \ll 1$ .

The equation for H<sub>2</sub> formation/dissociation is

$$\frac{df}{dt} = \mathcal{F}, \quad (\text{A6})$$

where  $\mathcal{F}$  is the net formation rate for H<sub>2</sub>.

By introducing new variables

$$x = \mu^{-1} = 1 - \frac{f}{2}, \quad (\text{A7})$$

---

<sup>5</sup> $f = 1$  corresponds to fully molecular.

$$\mathcal{P} = \mu_{\text{a}} \left[ \frac{2m_{\text{H}}\mathcal{L}}{3k_{\text{B}}T} - \frac{1}{3} \left( \frac{1}{2} + \frac{\chi}{k_{\text{B}}T} \right) \mathcal{F} \right], \quad (\text{A8})$$

and

$$\mathcal{Q} = \frac{\mathcal{F}}{2-f}, \quad (\text{A9})$$

the equations (A1) and (A6) can be written as

$$\frac{d\ln T}{dt} - \frac{2x}{x+2} \frac{d\ln \rho}{dt} + \mathcal{P} = 0 \quad (\text{A10})$$

and

$$\frac{d\ln x}{dt} + \mathcal{Q} = 0. \quad (\text{A11})$$

For perturbed quantities, we use the following notation:

$$\delta_T = \frac{\delta T}{T}, \quad \delta_\rho = \frac{\delta \rho}{\rho}, \quad \delta_x = \frac{\delta x}{x}. \quad (\text{A12})$$

The linear analysis is carried out under the isobaric condition  $\delta P = 0$ :

$$\delta_T + \delta_\rho + \delta_x = 0. \quad (\text{A13})$$

Perturbation of equation (A10) reads:

$$\frac{d\delta_T}{dt} - \left( \frac{2x}{x+2} \right) \frac{d\delta_\rho}{dt} + T\mathcal{P}_T\delta_T + \rho\mathcal{P}_\rho\delta_\rho + (x\mathcal{P}_x - \mathcal{R})\delta_x = 0, \quad (\text{A14})$$

where

$$\mathcal{R} = \frac{4x}{(x+2)^2} t_{\text{dyn}}^{-1}. \quad (\text{A15})$$

We define the dynamical timescale as

$$t_{\text{dyn}} = \left( \frac{d\ln \rho}{dt} \right)_{\text{bg}}^{-1} \quad (\text{A16})$$

for the collapsing background of the perturbation.

Perturbation of H<sub>2</sub> formation/dissociation equation reads:

$$\frac{d\delta_x}{dt} + T\mathcal{Q}_T\delta_T + \rho\mathcal{Q}_\rho\delta_\rho + x\mathcal{Q}_x\delta_x = 0. \quad (\text{A17})$$

We assume that  $\delta_T, \delta_\rho$ , and  $\delta_x \propto \exp(\omega t)$ . Seeking non-trivial solutions of equations (A13), (A14) and (A17) for  $\delta_T, \delta_\rho$  and  $\delta_x$ , we obtain the following equation for the growth rate of instability,  $\omega$ :

$$a_0\omega^2 + a_1\omega + a_2 = 0. \quad (\text{A18})$$

The coefficients are

$$a_0 = 1 + \frac{3}{2} \frac{\mu}{\mu_a}, \quad (\text{A19})$$

$$a_1 = \left( \frac{x+2}{2x} \right) [(T\mathcal{P}_T - \rho\mathcal{P}_\rho) + (x\mathcal{Q}_x - \rho\mathcal{Q}_\rho)] - (T\mathcal{Q}_T - x\mathcal{Q}_x) \quad (\text{A20})$$

$$= \frac{\mu m_H}{k_B T} (T\mathcal{L}_T - \rho\mathcal{L}_\rho - \mathcal{L}) - \frac{\mu\chi}{2k_B T} (T\mathcal{F}_T - \rho\mathcal{F}_\rho - \mathcal{F}) \quad (\text{A21})$$

$$- \left( 1 + \frac{3}{2} \frac{\mu}{\mu_a} \right) \left( \mathcal{F}_f + \frac{\mu}{2} \rho\mathcal{F}_\rho + \frac{\mathcal{F}}{2-f} \right) - \frac{3\mu}{4} (T\mathcal{F}_T - \rho\mathcal{F}_\rho), \quad (\text{A22})$$

and

$$a_2 = \left( \frac{x+2}{2x} \right) [(T\mathcal{P}_T - \rho\mathcal{P}_\rho)(x\mathcal{Q}_x - \rho\mathcal{Q}_\rho) - (T\mathcal{Q}_T - \rho\mathcal{Q}_\rho)(x\mathcal{P}_x - \rho\mathcal{P}_\rho - \mathcal{R})] \quad (\text{A23})$$

$$= -\frac{\mu m_H}{k_B T} (T\mathcal{L}_T - \rho\mathcal{L}_\rho - \mathcal{L}) \left( \mathcal{F}_f + \frac{\mu}{2} \rho\mathcal{F}_\rho + \frac{\mathcal{F}}{2-f} \right) \quad (\text{A24})$$

$$+ \frac{\mu m_H}{k_B T} \left( \mathcal{L}_f + \frac{\mu}{2} \rho\mathcal{L}_\rho + \frac{\mu_a}{6} \mathcal{L} \right) (T\mathcal{F}_T - \rho\mathcal{F}_\rho) \quad (\text{A25})$$

$$+ \frac{\mu}{2} \mathcal{F} \left[ \frac{\mu\mu_a}{3} \left( \frac{1}{2} + \frac{\chi}{k_B T} \right) (T\mathcal{F}_T - \rho\mathcal{F}_\rho) - \frac{\chi}{k_B T} \left( \mathcal{F}_f + \frac{\mu}{2} \rho\mathcal{F}_\rho + \frac{\mathcal{F}}{2-f} \right) \right] \quad (\text{A26})$$

$$+ \frac{\mu\mu_a}{3t_{\text{dyn}}} (T\mathcal{F}_T - \rho\mathcal{F}_\rho). \quad (\text{A27})$$

In the bottom panel of Figure 6, we plot the e-folding growth time of the instability  $t_e = \omega^{-1}$  for a collapsing primordial clump. The collapse rate is assumed to be free-fall,  $t_{\text{dyn}} = t_{\text{ff}} = \sqrt{3\pi/32G\rho}$ . The  $\text{H}_2$  line cooling rate is computed as in Omukai (2001), where the escape probability method is used for the cooling by optically thick lines. Also shown are the background temperature (*top*) and molecular fraction (*middle*) for the perturbation. We see from this figure that fluctuations grow by thermal instability, in other words, the thermal instability timescale,  $t_e$ , falls below the collapse timescale for the clump,  $t_{\text{ff}}$ , during the active phase of three-body  $\text{H}_2$  formation process. However, the ratio of the growth rate relative to the collapse rate,  $t_{\text{ff}}/t_e$ , remains below 2. Since the scale for thermal instability is  $\lambda_{\text{th}} \sim c_s t_e$  while the core size is approximately the Jeans length,  $\lambda_J \sim c_s t_{\text{ff}}$ , this means that the growing scale is larger than a half of the core size. Therefore, although the thermal instability does occur, it may only accelerate the collapse of the central region rather than driving further fragmentation.

Abel et al. (2000) investigated the collapse of a prestellar core by 3-D hydrodynamical simulation. In their calculation, the sub-fragmentation during the three-body  $\text{H}_2$  formation has not been observed. They interpreted this as a result of hypothetical turbulent mixing. Our argument here may give an alternative explanation of their result.

## REFERENCES

- Abel, T., Bryan, G. L., & Norman, M. L. 2000, *ApJ*, 540, 39
- Abel, T., Bryan, G. L., & Norman, M. L. 2002, *Science*, 295, 93
- Baraffe, I., Heger, A., & Woosley, S. E. 2001, *ApJ*, 550, 890
- Beers, T. C. 2003, *Nature*, 422, 825
- Bonifacio, P., Limongi, M., & Chieffi, A. 2003, *Nature*, 422, 834
- Bromm, V., Coppi, P. S., & Larson, R. B. 1999, *ApJ*, 527, L5
- Bromm, V., Coppi, P. S., & Larson, R. B. 2002, *ApJ*, 564, 23
- Bromm, V. & Loeb, A. 2003, *ApJin press* (astro-ph/0212400)
- Carlberg, R. G. 1981, *MNRAS*, 197, 1021
- Christlieb, N., Bessell, M. S., Beers, T.C., Gustaffson, B., Korn, A., Barklem, P.S., Karlsson, M., Mizuno-Wiedner, M., & Rossi, S. 2002, *Nature*, 419, 904
- Ciardi, B., Ferrara, A., Governato, F., & Jenkins, A. 2000, *MNRAS*, 314, 611
- Elmegreen, B. G., & Lada, C. J. 1977, *ApJ*, 214, 725
- Ezer, D., & Cameron, A. G. W. 1971, *Ap&SS*
- Franco, J., Tenorio-Tagle, G., & Bodenheimer, P. 1990, *ApJ*, 349, 126
- Fujimoto, M. Y., Ikeda, Y., & Iben, I., Jr. 2000, *ApJ*, 529, L25
- Glover, S. C. O., & Brand, P. W. J. L. 2001, *MNRAS*, 321, 385
- Hasegawa, T., Yoshii, Y., & Sabano, Y. 1981, *A&A*, 98, 186
- Haiman, Z., Thoul, A. A., & Loeb, A. 1996, *ApJ*, 464, 523
- Hoyle, F. 1953, *ApJ*, 118, 513
- Inutsuka, S. & Miyama, S. M. 1997, *ApJ*, 480, 681
- Kennicutt, R. C., Jr. 1998, *ARA&A*, 36, 189
- Kudritzki, R.-P. 2000 in *First Stars*, Proc. of the MPA/ESO workshop, eds. Weiss, A., Abel, T. G., & Hill, V., 127



- Machacek, M. E., Bryan, G. L., & Abel, T. 2001, *ApJ*, 548, 509
- Mackey, J., Bromm, V., & Hernquist, L. 2003, *ApJ*, 586, 1
- Matsuda, T., Sato, H., & Takeda, H., 1969, *Prog. Theor. Phys.*, 42, 219
- Miyama, S. M., Narita, S., & Hayashi, C. 1987a, *Prog. Theor. Phys.*, 78, 1051
- Miyama, S. M., Narita, S., & Hayashi, C. 1987b, *Prog. Theor. Phys.*, 78, 1273
- Nagasawa, M. 1987, *Prog. Theor. Phys.*, 77, 635
- Nakada, Y., & Yoneyama, T. 1976, *PASJ*, 28, 61
- Nakamura, F., & Umemura, M. 2001, *ApJ*, 548, 19
- Omukai, K. 2001, *ApJ*, 546, 635
- Omukai, K., & Nishi, R. 1998, *ApJ*, 508, 141
- Omukai, K., & Nishi, R. 1999, *ApJ*, 518, 64
- Omukai, K., & Palla, F. 2001, *ApJ*, 561, L55
- Omukai, K., & Palla, F. 2003, *ApJ*, 589, 677
- Palla, F., Salpeter, E. E., & Stahler, S. W. 1983, *ApJ*, 271, 632
- Sabano, Y. & Yoshii, Y. 1977, *PASJ*, 29, 207
- Saslaw, W. C., & Zipoy, D. 1967, *Nature*, 216, 976
- Schaerer, D. 2002, *A&A*, 382, 28
- Schneider, R., Ferrara, A., Natarajan, P., & Omukai, K. 2002, *ApJ*, 571, 30
- Schneider, R., Ferrara, A., Salvaterra, R., Omukai, K., & Bromm, V. 2003, *Nature*, 422, 869
- Shigeyama, T., Tsujimoto, T., & Yoshii, Y. 2003, *ApJ*, 586, L57
- Silk, J. 1977, *ApJ*, 214, 718
- Silk, J. 1983, *ApJ*, 205, 705
- Stahler, S. W., Palla, F., & Salpeter, E. E. 1986, *ApJ*, 302, 590
- Susa, H., & Kitayama, T., 2000, *MNRAS*, 317, 175

- Uehara, H., & Inutsuka, S., 2000, ApJ, 531, L91
- Uehara, H., Susa, H., Nishi, R., Yamada, M., & Nakamura, T. 1996, ApJ, 473, L95
- Umeda, H., & Nomoto, K., 2002, ApJ, 565, 385
- Umeda, H., & Nomoto, K., 2003, Nature, 422, 871
- Yoneyama, T. 1972, PASJ, 24, 87
- Yoshida, N., Abel, T., Hernquist, L., & Sugiyama, N., 2003, ApJ, 592, 645
- Yoshii, Y. 1981 A&A, 97, 280
- Yoshii, Y., & Sabano, Y. 1979, PASJ, 31, 505
- Yoshii, Y., & Saio, H. 1985, ApJ, 295, 521
- Yoshii, Y., & Saio, H. 1986, ApJ, 301, 587

Figures

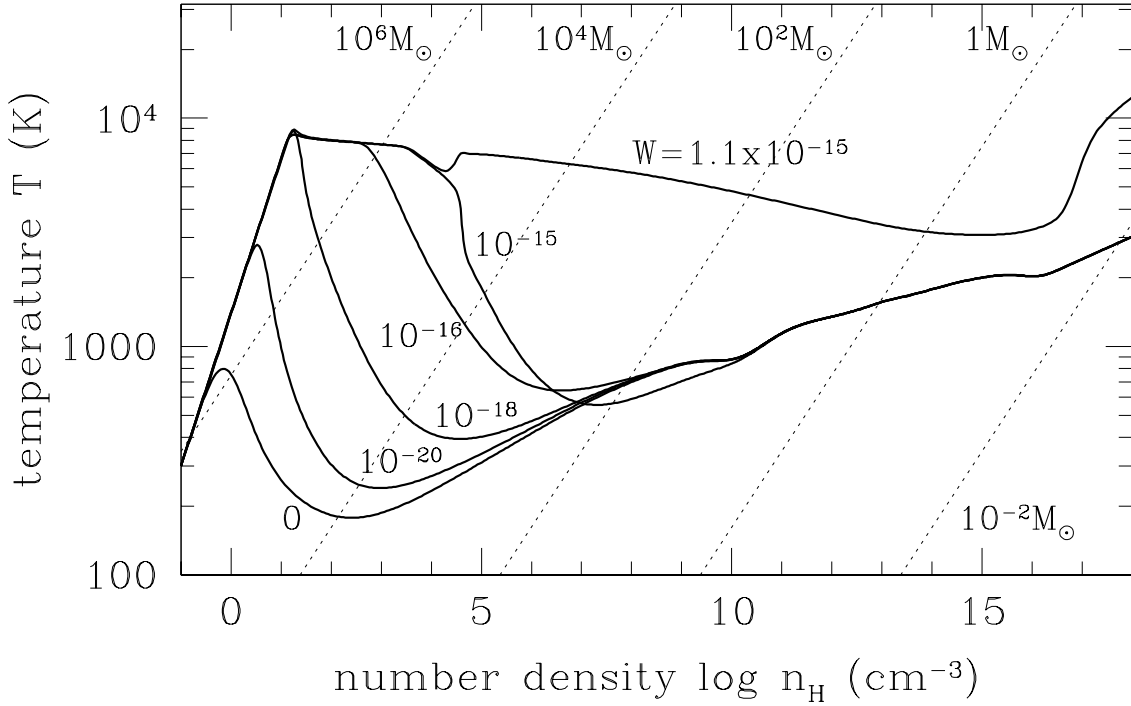


Fig. 1.— The temperature evolution for contracting metal-free prestellar clumps as a function of FUV radiation density. FUV radiation density is parameterized by the dilution factor  $W = u_{\text{rad}}/aT_{\text{rad}}^4$ , where  $T_{\text{rad}} = 10^5 \text{K}$ . The values of  $W$  are denoted in the figure. The collapse proceeds by  $\text{H}_2$  cooling for FUV radiation below the threshold  $W_{\text{noH}_2} \simeq 1.1 \times 10^{-15}$ . Whereas for  $W > W_{\text{noH}_2}$ ,  $\text{H}_2$  formation is prohibited by photodissociation, and the clump collapses by atomic cooling. The dashed lines indicate the constant Jeans mass.

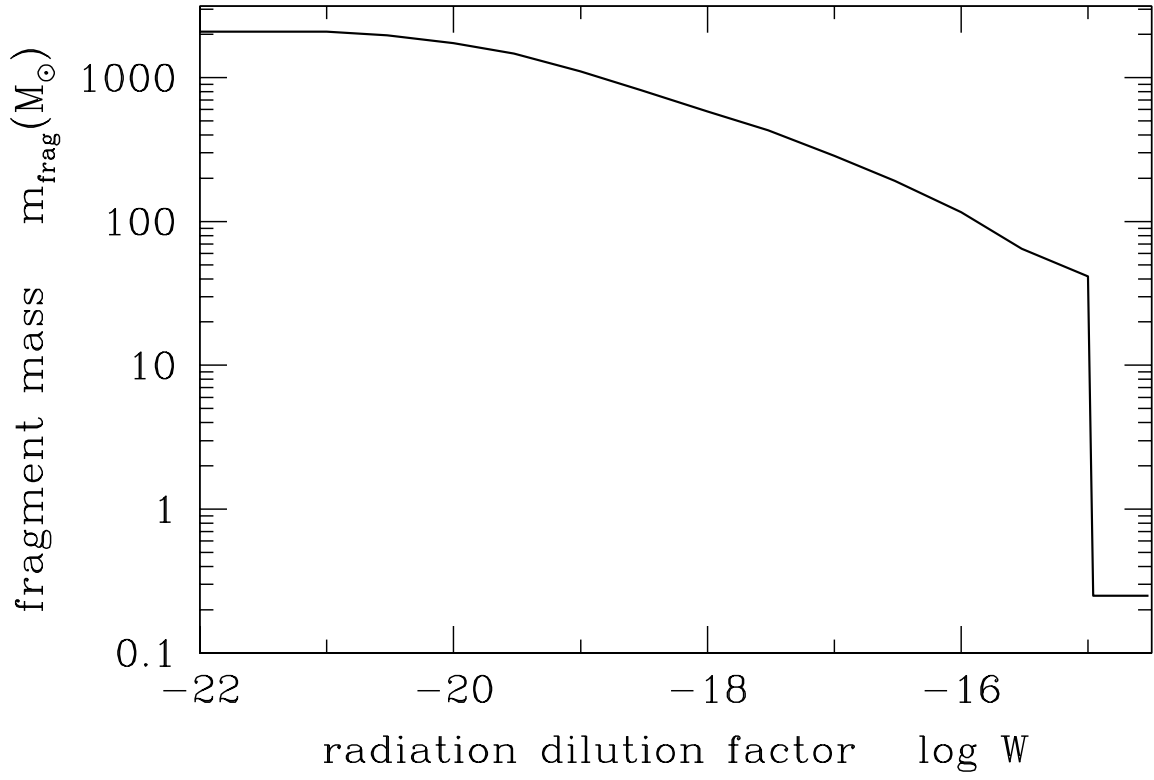


Fig. 2.— The fragmentation mass scale as a function of the dilution factor  $W$ , which parametrizes the FUV radiation density.

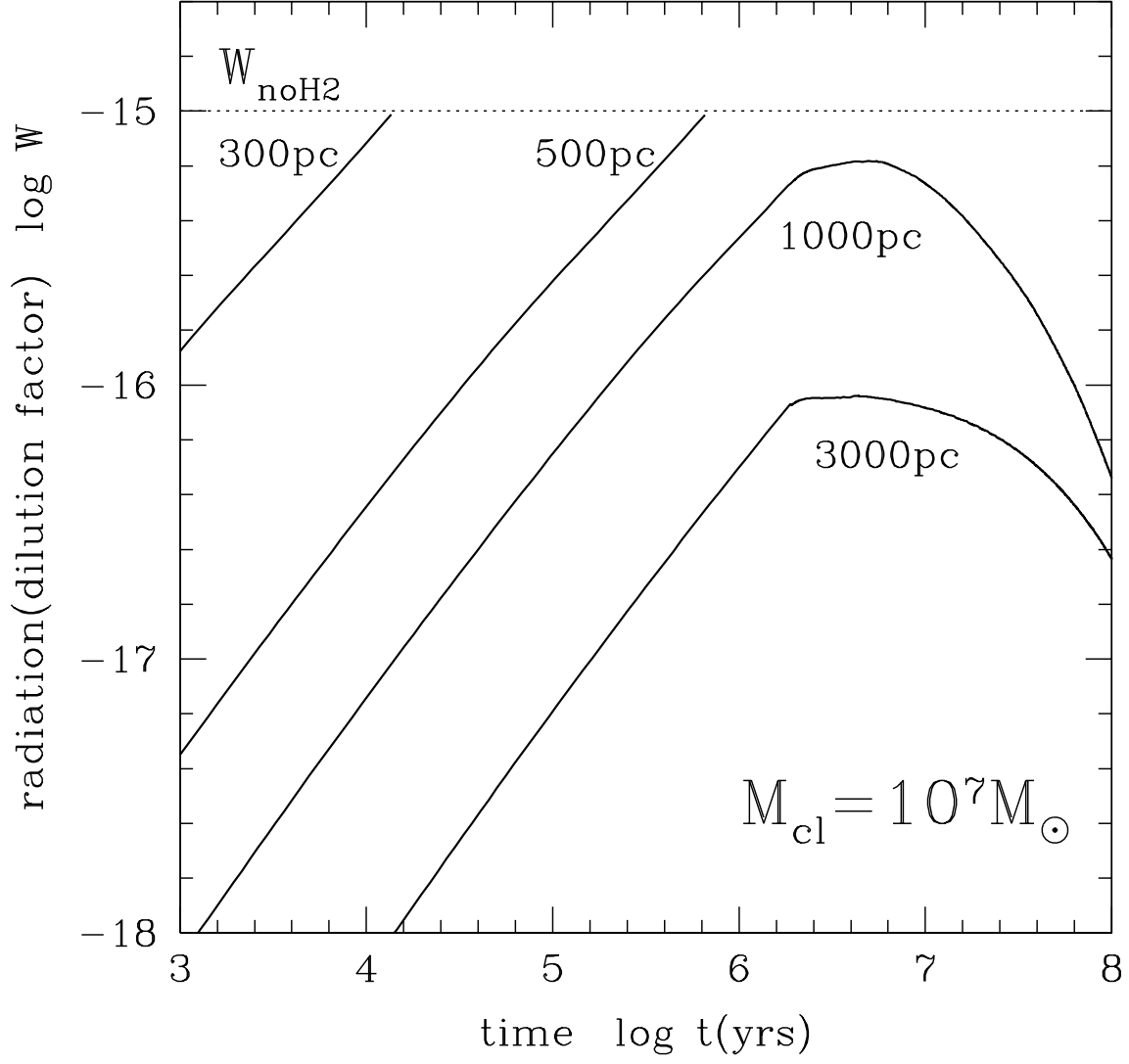


Fig. 3.— The evolution of FUV radiation density as a function of the cloud length scale. The initial gas mass of the clouds is  $M_{\text{cl}} = 10^7 M_{\odot}$ .

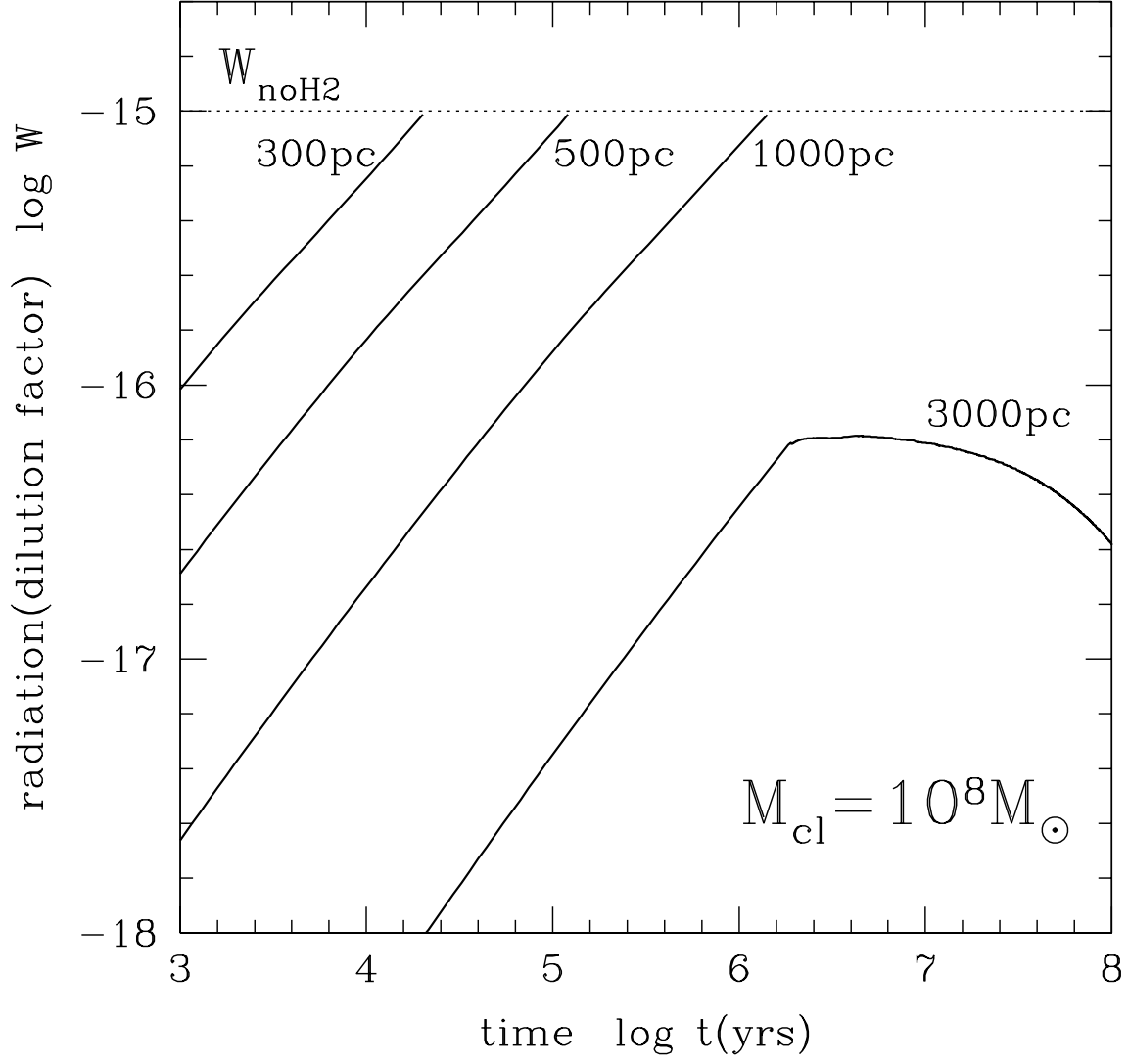


Fig. 4.— The same as Fig.3, but for the initial gas mass  $M_{\text{cl}} = 10^8 M_{\odot}$ .

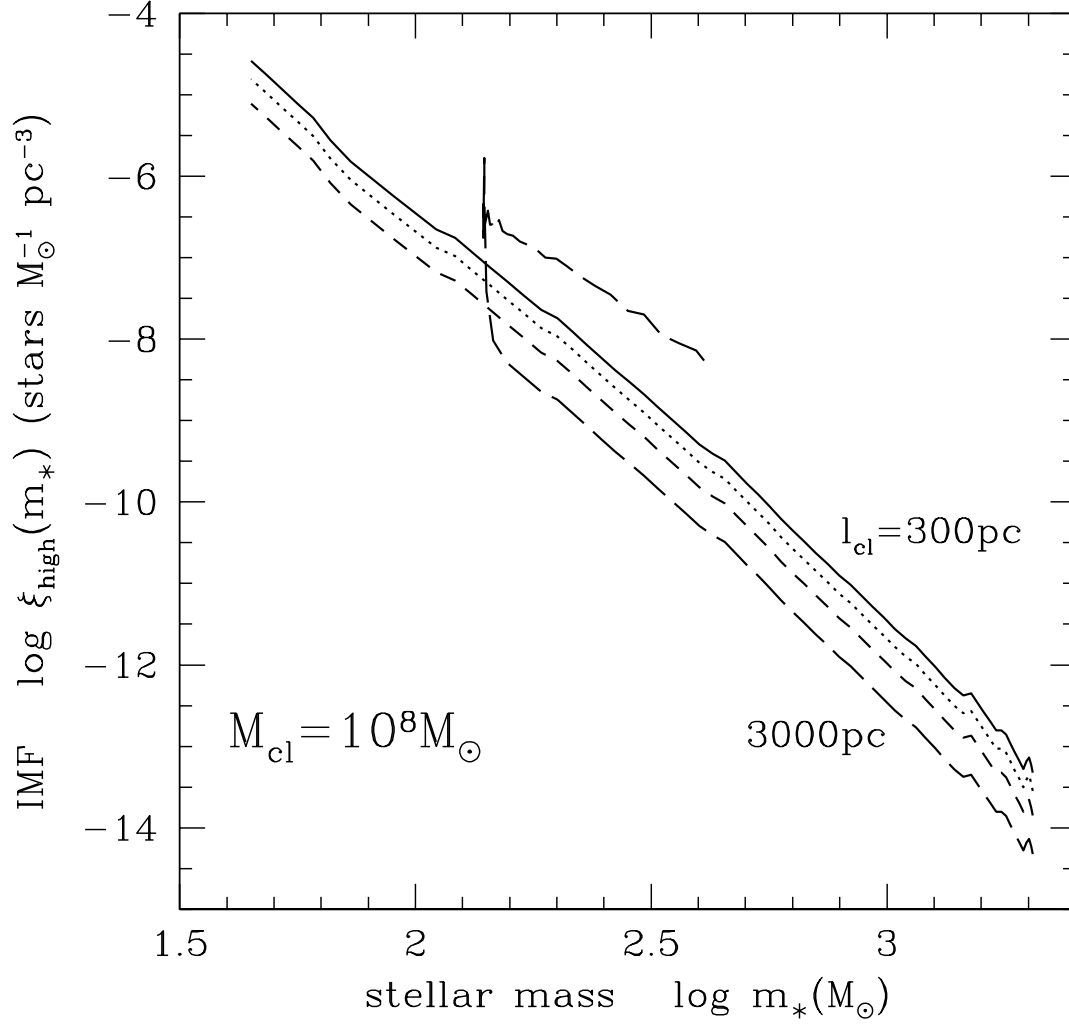


Fig. 5.— The initial mass function of metal-free stars in clouds of  $M_{\text{cl}} = 10^8 M_{\odot}$ . Shown are the results for the cloud length scale of 300pc (solid line), 500pc (dotted line), 1000pc (short-dashed line), and 3000pc (long-dashed line).

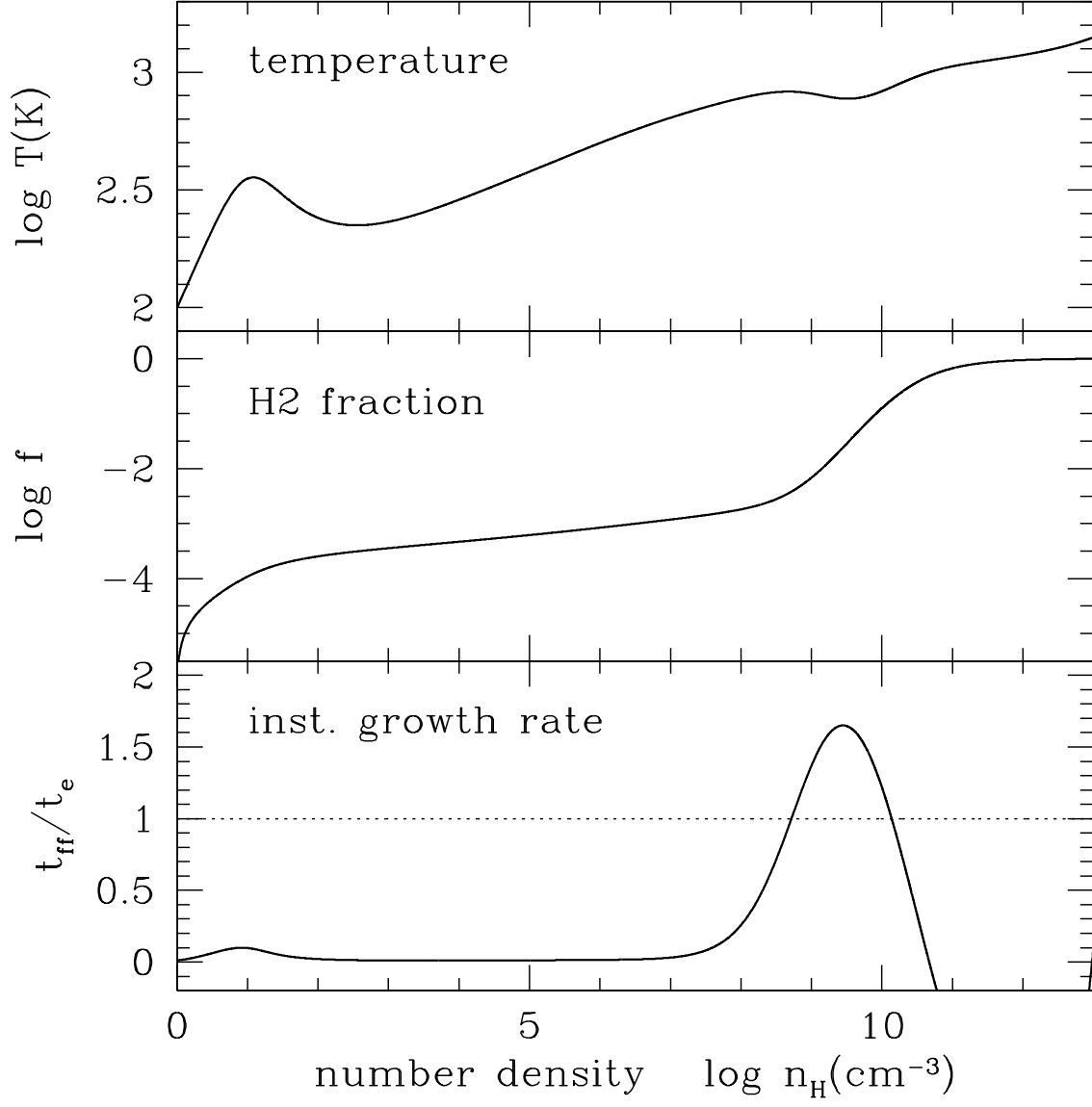


Fig. 6.— The growth rate of thermal instability ( $t_{\text{e}}^{-1} = \omega$ ) relative to the free-fall rate along the evolutionary path of the collapsing clump. Also shown are the gas temperature and H<sub>2</sub> fraction evolutions used as the unperturbed state of such clump.



p	3.11E-01	d	3.91E-08	<sup>3</sup> He	9.28E-07	<sup>4</sup> He	2.20E-01	<sup>6</sup> Li	1.05E-12
<sup>7</sup> Li	9.41E-11	<sup>9</sup> Be	2.62E-20	<sup>10</sup> B	2.21E-11	<sup>11</sup> B	9.48E-11	<sup>12</sup> C	1.24E-02
<sup>13</sup> C	1.32E-09	<sup>14</sup> N	9.07E-06	<sup>15</sup> N	3.42E-08	<sup>16</sup> O	6.53E-02	<sup>17</sup> O	9.72E-09
<sup>18</sup> O	1.78E-07	<sup>19</sup> F	9.00E-09	<sup>20</sup> Ne	5.28E-03	<sup>21</sup> Ne	6.53E-07	<sup>22</sup> Ne	1.20E-06
<sup>23</sup> Na	1.72E-05	<sup>24</sup> Mg	3.27E-03	<sup>25</sup> Mg	2.39E-06	<sup>26</sup> Mg	1.51E-06	<sup>26</sup> Al	5.16E-08
<sup>27</sup> Al	3.43E-05	<sup>28</sup> Si	4.44E-03	<sup>29</sup> Si	1.38E-05	<sup>30</sup> Si	3.77E-06	<sup>31</sup> P	2.23E-06
<sup>32</sup> S	1.87E-03	<sup>33</sup> S	4.59E-06	<sup>34</sup> S	1.54E-06	<sup>36</sup> S	1.34E-11	<sup>35</sup> Cl	3.66E-07
<sup>37</sup> Cl	3.50E-07	<sup>36</sup> Ar	3.09E-04	<sup>38</sup> Ar	3.77E-07	<sup>40</sup> Ar	1.48E-13	<sup>39</sup> K	1.15E-07
<sup>40</sup> K	1.41E-11	<sup>41</sup> K	3.85E-08	<sup>40</sup> Ca	2.74E-04	<sup>42</sup> Ca	6.58E-09	<sup>43</sup> Ca	1.89E-09
<sup>44</sup> Ca	2.00E-06	<sup>46</sup> Ca	3.97E-14	<sup>48</sup> Ca	8.60E-15	<sup>45</sup> Sc	1.75E-09	<sup>46</sup> Ti	6.86E-09
<sup>47</sup> Ti	3.03E-08	<sup>48</sup> Ti	4.98E-06	<sup>49</sup> Ti	8.81E-08	<sup>50</sup> Ti	1.25E-14	<sup>50</sup> V	5.29E-14
<sup>51</sup> V	6.63E-08	<sup>50</sup> Cr	4.60E-08	<sup>52</sup> Cr	4.70E-05	<sup>53</sup> Cr	1.82E-06	<sup>54</sup> Cr	1.37E-12
<sup>55</sup> Mn	2.25E-06	<sup>54</sup> Fe	7.04E-06	<sup>56</sup> Fe	2.79E-03	<sup>57</sup> Fe	4.77E-05	<sup>58</sup> Fe	5.61E-12
<sup>59</sup> Co	3.78E-07	<sup>58</sup> Ni	5.50E-06	<sup>60</sup> Ni	7.57E-05	<sup>61</sup> Ni	2.48E-06	<sup>62</sup> Ni	1.54E-06
<sup>64</sup> Ni	5.73E-14	<sup>63</sup> Cu	3.58E-08	<sup>65</sup> Cu	3.53E-08	<sup>64</sup> Zn	3.82E-06	<sup>66</sup> Zn	1.24E-07
<sup>67</sup> Zn	1.63E-10	<sup>68</sup> Zn	1.40E-09	<sup>70</sup> Zn	2.74E-14	<sup>69</sup> Ga	2.01E-10	<sup>71</sup> Ga	9.98E-14
<sup>70</sup> Ge	4.51E-10	<sup>72</sup> Ge	2.11E-13	<sup>73</sup> Ge	1.05E-13	<sup>74</sup> Ge	6.10E-14		

Table 1: The mean ejected mass fraction of element X,  $\epsilon_{X,\text{high}}$ , in the case of the transition mass  $m_{\text{tr}} = 20M_{\odot}$ . The mean remnant mass is  $\alpha_{\text{high}} = 0.379$

p	3.58E-03	d	9.53E-11	<sup>3</sup> He	4.84E-09	<sup>4</sup> He	4.36E-03	<sup>6</sup> Li	2.35E-20
<sup>7</sup> Li	1.69E-13	<sup>9</sup> Be	7.85E-20	<sup>10</sup> B	2.14E-19	<sup>11</sup> B	6.49E-14	<sup>12</sup> C	3.21E-04
<sup>13</sup> C	7.82E-10	<sup>14</sup> N	6.68E-07	<sup>15</sup> N	2.09E-08	<sup>16</sup> O	4.40E-03	<sup>17</sup> O	1.86E-08
<sup>18</sup> O	8.13E-08	<sup>19</sup> F	2.33E-11	<sup>20</sup> Ne	2.33E-04	<sup>21</sup> Ne	3.21E-08	<sup>22</sup> Ne	6.18E-08
<sup>23</sup> Na	6.28E-07	<sup>24</sup> Mg	2.38E-04	<sup>25</sup> Mg	2.39E-07	<sup>26</sup> Mg	7.67E-08	<sup>26</sup> Al	9.99E-09
<sup>27</sup> Al	2.19E-06	<sup>28</sup> Si	1.34E-03	<sup>29</sup> Si	1.94E-06	<sup>30</sup> Si	2.19E-07	<sup>31</sup> P	1.76E-07
<sup>32</sup> S	7.43E-04	<sup>33</sup> S	8.74E-07	<sup>34</sup> S	1.80E-07	<sup>36</sup> S	1.82E-12	<sup>35</sup> Cl	7.20E-08
<sup>37</sup> Cl	1.72E-07	<sup>36</sup> Ar	1.24E-04	<sup>38</sup> Ar	1.47E-07	<sup>40</sup> Ar	9.46E-15	<sup>39</sup> K	4.24E-08
<sup>40</sup> K	1.38E-12	<sup>41</sup> K	2.65E-08	<sup>40</sup> Ca	1.20E-04	<sup>42</sup> Ca	4.05E-09	<sup>43</sup> Ca	1.92E-09
<sup>44</sup> Ca	5.47E-08	<sup>46</sup> Ca	5.65E-14	<sup>48</sup> Ca	4.50E-17	<sup>45</sup> Sc	2.35E-09	<sup>46</sup> Ti	2.44E-09
<sup>47</sup> Ti	1.79E-09	<sup>48</sup> Ti	5.20E-07	<sup>49</sup> Ti	1.75E-08	<sup>50</sup> Ti	1.90E-16	<sup>50</sup> V	4.76E-15
<sup>51</sup> V	1.44E-08	<sup>50</sup> Cr	3.95E-08	<sup>52</sup> Cr	9.19E-06	<sup>53</sup> Cr	4.73E-07	<sup>54</sup> Cr	4.12E-12
<sup>55</sup> Mn	1.58E-06	<sup>54</sup> Fe	1.55E-05	<sup>56</sup> Fe	3.31E-04	<sup>57</sup> Fe	4.32E-06	<sup>58</sup> Fe	3.54E-11
<sup>59</sup> Co	1.39E-07	<sup>58</sup> Ni	1.32E-05	<sup>60</sup> Ni	1.23E-06	<sup>61</sup> Ni	8.15E-09	<sup>62</sup> Ni	3.01E-08
<sup>64</sup> Ni	4.28E-16	<sup>63</sup> Cu	2.14E-10	<sup>65</sup> Cu	1.34E-11	<sup>64</sup> Zn	1.42E-09	<sup>66</sup> Zn	2.41E-10
<sup>67</sup> Zn	5.82E-13	<sup>68</sup> Zn	1.92E-13	<sup>70</sup> Zn	3.24E-16	<sup>69</sup> Ga	4.01E-14	<sup>71</sup> Ga	8.33E-16
<sup>70</sup> Ge	8.42E-13	<sup>72</sup> Ge	1.49E-15	<sup>73</sup> Ge	1.08E-15	<sup>74</sup> Ge	3.55E-16		

Table 2: The same as Table 1, but for the transition mass  $m_{\text{tr}} = 40M_{\odot}$ . The mean remnant mass fraction  $\alpha_{\text{high}} = 0.984$

[X/Fe]	Li	C	N	O	Na	Mg	Ca	Ti	Ni	Zn
HE 0107-5240	< 5.3	4.0	2.3	2.4	0.8	0.2	0.4	-0.4	-0.4	< 2.7
$m_{\text{tr}} = 20M_{\odot}$	-3.28	-0.41	-3.03	-0.06	-1.02	-0.02	0.16	-0.17	-0.26	0.00
$m_{\text{tr}} = 25M_{\odot}$	-4.43	-0.49	-3.21	-0.05	-1.12	0.00	0.18	-0.18	-0.26	-0.08
$m_{\text{tr}} > 30M_{\odot}$	-5.12	-1.09	-3.25	-0.32	-1.55	-0.25	0.70	-0.23	-0.12	-2.46

Table 3: Comparison of abundance ratios [X/Fe] with HE 0107-5240